Slow waves in locally resonant metamaterials line defect waveguides

Nadège Kaina[1], **Alexandre Causier**[2], **Yoan Bourlier**[2], **Mathias Fink**[1], **Thomas Berthelot**[2], **Geoffroy Lerosey**[1]

[1] *Institut Langevin, ESPCI ParisTech & CNRS, Paris, France*

[2] *CEA Saclay, IRAMIS, NIMBE, LICSEN, UMR 3685, F-91191, Gif sur Yvette, France*

The ability of electromagnetic waves to interact with matter governs many fascinating effects involved in fundamental and applied, quantum and classical physics. It is necessary to enhance these otherwise naturally weak effects by increasing the probability of wave/matter interactions, either through field confinement or slowing down of waves. This is commonly achieved with structured materials such as photonic crystal waveguides or coupled resonator optical waveguides. Yet their minimum structural scale is limited to the order of the wavelength which not only forbids ultra-small confinement but also severely limits their performance for slowing down waves. Here we show that line defect waveguides in locally resonant metamaterials can outperform these proposals due to their deep subwavelength scale. We experimentally demonstrate our approach in the microwave domain using 3D printed resonant wire metamaterials, achieving group indices n_g as high as 227 over relatively wide frequency bands. Those results correspond to delay-bandwidth products, one of the slow wave devices figure of merit, 10 times higher than any proposal based on structured materials. We further prove that the delay-bandwidth product of metamaterial line defect waveguide is inversely proportional to the typical spatial scale of these composite media, a property that is unique to their resonant nature. Our findings, though demonstrated in the microwave domain for a specific structure, are very general and can be transposed to various resonant unit cells, frequency range and even other types of waves such as acoustic or elastic ones.

INTRODUCTION

Enhancing the ability of waves to interact with matter is a prerequisite for many promising applications. In optics for instance, it can benefit low-power non linear physics[1], efficient solar energy harvesting[2], miniature lasers[3] or be used to control the spontaneous emmision rate of atoms[4]. At lower frequencies on the other hand, from the near infrared to microwave frequencies, or for surface acoustic waves, it can be required for analog information processing, cavity QED or detection of hazardous products.

Maximizing the probability of wave interactions with a given medium requires two achievements to be met: first the wave needs to be strongly confined to locally enhance the field energy density in the medium of interest and second it has to be slowed down to extend the interaction time. Photonic and Phononic crystals[5] are considered as natural candidates for both slow-wave[6–8] and strong field confinement[5,9], due to their ability to support defect cavities and line defect waveguides. Yet these Bragg interference based media, whose properties rely mainly on their structure, are by definition wavelength scaled. This sets several constraints. First of all, they obviously cannot be used as compact components at lower frequencies, as in the microwave domain. Then, even at optical frequencies, this scale sets a lower limit to the spatial confinement they can achieve and imposes that slow wave propagation always comes at the expense of a bandwidth narrowing[10]. The second common implementation of slow waves is through the exploitation of the strong dispersion brought by resonances, either through an electromagnetic induced transparency window[11,12] or with coupled resonators optical waveguides[13–15] (CROWs) as it is the case for coupled photonic crystals cavities[16,17]. However, these proposals also present the fundamental limitation that using extremely resonant materials or very high quality factor resonators again severly restricts the frequency range over which waves can be slowed down. The efficiency of slow wave devices can hence be characterized by the normalized delay-bandwidth product (NDBP), a dimensionless figure of merit independent of the length of the device, underlining how broadband the latter can operate given its slowing 'strength', i.e. its group index n_g. It is defined as NDBP= $v_g/c*\Delta f/f_0=n_g*\Delta f/f_{0,}$ where Δf is the bandwidth and f_0 the central frequency of the device. In all photonic crystal/CROWs based slow wave devices, this NDBP is intrinsically limited: the slower the wave, the narrower the bandwidth[18]. Though efforts have been made to overcome this limitation, for instance by inducing adiabatic tuning of the device[19] or 'chirping' its properties[20], NDBP typical values remain less than unity.

In this article, we investigate how these constraints can be released by transposing the previous slow wave concepts into the metamaterial field. Metamaterials, that are composite media generally composed of resonators organized at deep-subwavelength scales, indeed present effective properties that can be very high, a property that was used to image or focus waves below the diffraction limit[21–27], or negative. In a previous work[28], we evidenced that this negative effective property can also be understood as a bandgap, resulting from the interference between the plane waves propagating in air and the locally resonant fields radiated by its elements. This purely interference based interpretation of the origin of the metamaterials bandgap, that emphasizes analogies with the physics of photonic crystals, allowed us to demonstrate that local modifications of the material induce, analogous to

photonic crystals, defects cavities able to confine the waves to the defect region. Contrarily to photonic crystal however, for which the bandgap is created by Bragg interferences on the periodic structure[29,30], and hence the defects are structural ones with sizes the order of the wavelength, the hybridization bandgap in metamaterial mainly stems from the resonant nature of its constituents. Defect cavities then typically consist in modifying the resonance frequency of one element so that it falls within the hybridization bandgap of the surrounding medium. It results in wave confinements on much smaller dimensions than in photonic crystal and in very high Purcell factors[31], due to the typical deep sub-wavelength metamaterial scales. Following this idea, it was further proved that inserting sequences of those resonant defects enables the creation of waveguides that can mold the flow of waves, again at deep subwavelength scales[28,32]. Through these studies, metamaterials appear as promising candidates to develop compact components with deep subwavelength field confinement, which is the first requierement for efficient wave-matter interaction.

Going beyond these results, dedicated only to the spatial control of the wave propagation, we now focus on the temporal properties of line defects waveguides in locally resonant metamaterials. We prove that they can slow down wave very effectively while largely outperforming slow wave devices based on structured materials in terms of delay-bandwidth products, owing to their deep subwalength scale. This in turn meets the temporal expectations for increased wave-matter interaction.

To do so, we study microwave samples based on arrays of quarter-wavelength resonant metallic wires, of given height L, sitting on a ground plane. For a defect created by shortening a wire to a length L_d (or equivalently increasing its resonance frequency[28]), this collection of resonators acts as a bandgap medium. By shortening several adjacent wires along a line, a metamaterial line defect waveguide is inserted, for which we measure both the temporal and spectral properties. Doing so, we experimentally evidence that slow waves propagate in the waveguides with group indices as high as $n_g = 227$, a value tunable through modifications of the geometric properties of the surrounding bandgap medium. Strikingly, we observe NDBP at least one order of magnitude higher than proposals from the photonic crystal community[33]. More importantly, we show that the NDBP is no longer limited, as in structured media such as PC or CROWs, but can be easily increased by tailoring the density of the metamaterial line defect waveguides. We confirm this property via simulations and prove that the NDBP evolves as the inverse of the metamaterial typical spatial scale, independantly of the wavelength, a property unique to the resonance driven physical mechanism of these media.

RESULTS

Slow microwave in a tortuous waveguide. To first explore the characteristics of the propagation in such metamaterial line defect waveguides, we manufacture, using a 3D printing process followed by a chemical wet copper plating (see SI), a periodic subwavelength square array (period a = 5 mm ~ λ_0/13) of L = 16 mm long copper-plated wires mounted on a ground plane. Such wires have a resonance frequency around f_0 = 4.5 GHz, so that this medium opens a bandgap above f_0[28]. The waveguide is then designed by replacing the wires along a tortuous path with L_d = 14 mm long defect wires, as depicted in the picture Figure 1a. To measure the waveguide properties, the latter is first fed by two home-made input and output antennas each plugged to a network analyzer. Those antennas are designed to be impedance matched to the defect wires to maximize the coupling to the waveguide and avoid reflections (see SI). The spectral transmission (Fig. 1c) highlights on the one hand the sudden drop of transmission above f_0, corresponding to the bandgap created by the long wires, and on the other hand a transmission band of 6% bandwidth (Δf = 300 MHz) around a central frequency f_c = 4.88 GHz, close to the defects resonance frequency. This band can be attributed to the presence of the line defect waveguide, as the spectral transmission of an array of all identical wires only displays a bandgap for this frequency range[28] (see SI). To assess the defect line indeed acts as a waveguide, we record the electric field by scanning the medium over a wide frequency range with a home-made antenna mounted on a 2D moving stage, while the antenna at the output port of the waveguide is plugged in to a standard 50 Ω load (see SI). A map of one of the modes (Fig. 1b) highlights the effective deep subwavelength confinement of the electric field around the defect wires (white circles) that is limited by the distance to the first neighbors in the surrounding medium (black circles), twice the period, i.e. λ_0/6.5. This confirms our first experiments[28] and further demonstrates that waves can be molded along arbitrary complex paths. Note that the transmission spectrum is not completely flat, as we could have expected using impedance matched antennas. This is due to some small reflections that are experienced by the wave around the numerous corners of this meandering propagation path. Those can be minimized though by adapting the waveguide geometry around the bends, as in photonic crystal waveguides[34]. Finally, the delay, or equivalently the group velocity of the microwaves propagating in the guide, can be estimated. To do so, a 20 MHz wide pulse centered aroud f_c is sent in the input antenna and measured at the output antenna (Fig. 1d), after a 55 ns delay due to the propagation through the L_g = 29.5 cm long meandering waveguide. This delay, equivalent to a propagation on 16.5 m in air, corresponds to a group index n_g =

56, and hence demonstrates that the wave is strongly slowed down in the metamaterial defect waveguides.

Origin of the slow wave propagation. To understand the origin of this very high group index and determine if it can be further enhanced, it is necessary to understand the physics underlying the propagation of waves in these line defect waveguides. The shorter wires constituting the waveguides are resonant defects within the bandgap created by the resonance of the otherwise longer wires of the surrounding metamaterial. The field is then necessarily tightly confined around each defect. The subwavelength transverse size of the waveguide furthermore proscribes the presence of propagating waves. Each of these defects can hence only be, in first approximation, evanescently coupled to its neighbors, with a coupling strength κ, so that waves tunnel from defect to defect through a tight-binding like interaction. The coupling strength, depending both on the field confinement around each defect and the distance between them (the two characteristics that affect the tunneling efficiency), partly determines the group velocity of the wave propagating in the defect waveguide. Indeed, the lower the coupling, i.e. the more difficult the tunneling, the slower the propagation and the higher the group index n_g. This mechanism is very similar to that of CROWs in optics[35], which have been experimentally realized using ultra-high Q cavities such as ring resonators[36,37] or defect cavities in photonic crystals[17,38]. Yet metamaterials are structured at deep subwavelength scales, much smaller than that of CROWs whose resonant elements can be several wavelengths large, or even that of photonic crystals waveguides which are typically wavelength scaled. We will see that this feature considerably enhances the slowing properties of these waveguides and especially their corresponding NDBP. The main question is then how to further increase the group index n_g. Since the velocity is partially driven by the coupling strength, the idea is to modulate κ, while acting first on the evanescent field confinement, which is set by the bandgap attenuation efficiency. Modifying the latter can for instance be achieved by adjusting the surrounding medium density. Indeed, the denser the bandgap medium is, the more efficient the bandgap attenuation becomes (Fig. 2a). The field around the defects in the line waveguide is then more tightly confined, decreasing the coupling strength κ and resulting in slower group velocities. Note that such a modification of the medium's structure is an unique advantage offered by metamaterials, since they are subwavelength scaled and governed by a local resonance rather than by Bragg interference as in PCs. These structured media indeed have a determined periodicity which is constrained by the wavelength and cannot be freely scaled without scaling the operating frequency as well.

Tuning n_g through the modification of the defect-defect tunneling. For the sake of simplicity, the group velocity tailoring is now demonstrated in straight waveguides. They are composed of 60 of the previous defect wires separated by a_g = 1.5 mm ~ $\lambda_0/40$ while the surrounding medium's wires are packed in a periodic array of lattice constant a varying from 5 mm to 2 mm in the four investigated samples (Fig. 2a), corresponding to periodicities ranging from $\lambda_0/13$ to $\lambda_0/30$. We first implement temporal measurements in order to characterize the group velocity in our waveguides. For each sample we send a 20 MHz wide pulse centered on the transmission band central frequency and measure the temporal delay achieved by the line defect waveguides (Fig. 2b). The results evidence that shrinking the medium periodicity from a = 5 mm to a = 2 mm indeed strongly modulates the delay, that extends from 20 ns to 68 ns corresponding to group indices from n_g = 65 to n_g = 227. This strong delay is equivalent to free space propagation of 5.8 m to 20.4 m, although the waveguide physical length is only L_g = 9 cm. Such high n_g is already as good as the best performances obtained in photonic crystal based slow light devices. Interestingly, the group index presents a linear dependance on the inverse of the medium density a^2 (Fig. 2c) and is hence highly tunable and improvable, since a is theoritically solely limited by the minimum spacing between the wires, that is their radius. After succesfully proving the group velocity tailoring, it is important to determine how the transmission bandwidth is affected by the velocity reduction, which is a natural concern regarding slow wave propagation. The measured transmission spectra for each waveguide (Fig. 2d) show that while increasing a, i.e. increasing the group index, the transmission bandwidth accordingly shrinks from Δf = 610 MHz to Δf = 250 MHz, that is from 10% to 2% of the central frequency. This is not surprising since in a tight-binding model, the bandwidth Δf of the band of propagating waves is directly proportionnal to the coupling strength κ. As we decreased κ to slow down the wave, through the surrounding medium density, the bandwidth is naturally highly impacted. Note that for this linear geometry of waveguides, the transmission bandwidths are flat, confirming the impedance matching of the antennas.

Delay-bandwidth products in locally resonant metamaterial based line defects waveguides. Despite this bandwidth reduction, one substantial observation is that these Δf remain very large compared to what can be obtained in photonic crystals or CROWs conventionnal slow wave devices. This is made particularly clear while calculating the corresponding NDBP for each waveguide, ranging from 7.5 (a = 5 mm) to 10.6 (a = 2 mm), values more than 10 times higher than any prior proposition based on CROWs or PC. This is a direct consequence of the deep subwavelength nature of the metamaterials, as evidenced in the scheme of Figure 3. In this figure, we represent the schematic sinusoidal dispersion

relation typical of tight-binding interactions, with a given coupling strength κ (i.e. a fixed bandwidth) for two linear chains of defects with different inter-spacing distance a_g between the defects : in the first one, this distance is typically of the order of the wavelength as it is the case in photonic crystal/ CROWs (blue) while in the second one, it is deeply subwavelegth, corresponding to our metamaterial defect line waveguide configuration (red). As the wavenumbers that can be reached in the waveguide are only governed by the edge of the first Brillouin zone that is π/a_g, our defect line waveguides support much higher wavenumber modes than other structured media based slow wave devices. This implies, as stated by the definition of the group index $n_g = c*\delta k/2\pi\delta f$, that for a given bandwidth (related to δf, the bandwidth variation, and driven by κ), the δk, and hence the group index, can be much higher in metamaterials. This is geometrically observable in the difference of slopes in the dispersion relations around the central frequency f_c (Fig. 3).

From the measurements, we observe that the NDBP, though slightly increasing, is far from being on a par with the large group index modulation. This can easily be understood considering that the NDBP = $n_g*\Delta f/f_0$ and the n_g modulation is more or less compensated by the bandwidth shrinking. For a tight-binding based propagation indeed, assuming that total bandwidth Δf is simply proportional to the linear effective bandwidth δf, the definition of the group index $n_g = c*\delta k/2\pi\delta f$ leads to NDBP ~ $c*\delta k/f_0$. In this case, the NDBP is then independent of the bandwidth of the device and is solely proportional to the wavenumber of the modes propagating in the line defect waveguide. This explains why this quantity is restricted to small and relatively constant values in PC or CROWs based structures, because the wavevector is constrained by the wavelength.

In our case, the small variation in the NDBP can be attributed to a slight deviation from the tight-binding model that is highlighted by the experimental determination of the dispersion relations of the wave propagating in the waveguides (see SI for protocol). Indeed, having a closer glimpse at those dispersion curves (Fig. 2e), we see that they are not purely sinusoidal, as expected in CROWs for instance, especially for the largest densities. This highlights that the propagation mechanism, while remaining principally tight-binding, also takes into account a small propagative part whose contribution depends on the strength of the field confinement around the defects. It gets more important when the bandgap attenuation efficiency is decreased, leading to dispersion relations presenting some features of a polariton, that is the dispersion relation that is expected when the defects are solely coupled through a propagating wave. Beyond these propagation mechanism considerations, we observe that these curves further confirm the group index modulation through the change in the slope around the central

frequency. As expected, the waveguides are highly dispersive hence practically limiting the effective bandwidth, as it is the case in all slow wave devices. We can however stress that the dispersion is linear over quite a wide range of frequencies around the central frequency, in agreement with the principal tight-binding contribution. It is for instance of interest for dispersionless broadband pulse propagation. This differs drastically from spoof plasmon based slow wave approaches for which the field is less confined and the group index very dispersive on the flat band edge of the polariton dispersion relation[39–42].

Despite the small increase of the NDBP while increasing the surrounding medium density, it remains relatively limited, due to the drastic bandwidth reduction. This leads to the following question: can the NDBP be further enhanced or, in other words, can the group index be largely increased while limiting the bandwidth shrinking? In the previous samples, we only tuned the group index via the coupling strength κ, i.e. via the bandwidth δf but a_g, and hence δk, remained constant, and so did the NDBP, as in structured media. Contrarily to the latter however, the wavenumber δk in metamaterials can be as well adjusted, providing a second lever that directly impacts the NDBP, which is what we demonstrate in the following sections.

Enhanced delay-bandwidth products through wavenumber modifications. To modulate the wavenumber of the modes within the waveguide, we again take advantage of metamaterial's unique properties that are independent of the spatial structuration to now modify the density of defects, that is a_g. Decreasing this period indeed leads to higher wavenumbers, and this consequently increases the group index. However, putting the defects closer also has one opposite consequence on the velocity: it facilitates the propagation through the augmentation of the coupling strength, hence decreasing the group index. As we previously demonstrated though, this coupling can as well be controlled by the surrounding medium wires' density independently of the waveguide geometrical parameters. In order to limit the impact of the waveguide density on the coupling strength, we propose to implement a scaling of the device's dimensions that amounts to simultaneously modifying the medium density (as in the previous paragraph) and the waveguide lattice constant. We then manufacture two components (Fig. 4a); the reference component ($S_c = 1$) is a straight waveguide with the transverse dimensions a = 10 mm ($\lambda_0/6.5$) for the medium and a_g = 6.97 mm ($\lambda_0/8.5$) for a 18 cm long waveguide. The second one ($S_c = 0.5$) has a and a_g reduced by half and the guide is then twice shorter. The spectral and temporal measurements, obtained following the same experimental procedure as previously, demonstrate a striking result. While with this scaling operation the group delay is multiplied by a factor 2.4, the

transmission bandwidth reduces only by 25% (Fig. 4b,c,e,f). This value is far beyond the 50 % bandwidth reduction for an equivalent slowing strength when the coupling strength κ is alone modulated keeping the wavenumber constant (Fig. 2d). As a direct consequence of the increase of the wavenumber δk of the slow wave modes, resulting from the geometrical scaling of the metamaterial, the NDBP is then multiplied by a factor 1.7, going from 4 to 7.5. This result completely overcomes the previous preconception of a systematic dramatic bandwidth reduction for large delay propagation in very slow wave components.

To complete the study, we again experimentally measure the dispersion relations and compare it with the theoretical tight-binding ones. As for the previous waveguides, we observe a slight deviation that can be attributed to a partly polaritonic-like behavior. This happens particularly for the Sc = 0.5 sample for which the smaller period in the waveguide may not completely prevent from direct propagative coupling. This could be avoided by decreasing the coupling between neighbors that is with higher medium density samples or larger periodicities in the waveguide.

Delay-bandwidth as a function of the metamaterial spatial scale. To confirm these experimental results, we finally prove that the scaling operation can be further implemented and that the denser we scale the metamaterial samples, that is the larger the wavenumber of the modes are, the higher the delay-bandwidth products are. Because our fabrication process has a limited resolution imposed by our 3D printer, we simulate, using the software CST microwave studio, twelve of the previous devices with scaling factor ranging from Sc = 2 to Sc = 0.125. We observe the same trend as in experiment: while the normalized transmission bandwidth shrinks by a factor of 6, from 18% to 3% of the central frequency, when Sc decreases (Fig. 5a,b), the group index increases by more than two orders of magnitude (Fig. 5b). This results in a NDBP with very large values, up to 16, that seems to follow a linear dependence to a power of Sc close to -1 (Fig. 5c). It is consequently far from being limited to constant values. Again, we explain this by the fact that the NDBP value principally depends on the wavenumber of the waves propagating in the waveguide. The slight difference from the expected power -1 could be the consequence of the deviation of our dispersion relation from the pure tight-binding one that introduces a small dependence of the NDBP on the bandwidth. Hence, using deep subwavelength scale metamaterials to create very dense line defect waveguides permits to obtain unprecedented NDBP. Note again that such a scaling operation is simply impossible to realize with other structured media such as photonic crystals or CROWs since their spatial scale imposes their operating frequency, hence setting a fixed maximum value for δk. Using composite media made out of resonant unit cells seems therefore a

very promising way to slow down waves, at least in areas where deep subwavelength and low loss ones are available.

DISCUSSION

To conclude, we demonstrated a new approach to slow down waves based on metamaterial subwavelength line defect waveguides. Owing to the subwavelength structuration of the metamaterials, we were able to demonstrate both very large group indices, here experimentally up to 227 and numerically up to 600, over relatively large operating bandwidths. As a consequence, we measured unprecedented normalized delay-bandwidth products, more than one order a magnitude higher than prior propositions based on structured materials and which can be further increased by a simple scaling of the physical dimensions of the devices. We believe that our concept that achieves both extremely high confinement and overcomes the current limitations related to the delay-bandwidth product of slow wave devices will be of great interest in many fields of research relying on wave/matter interactions. It also paves the way to the design of ultracompact components that spatially and temporally control the propagation of waves at scales independent of the wavelength. Finally, we would like to emphasize that our approach is very general and can be applied to other frequency ranges, with other kind of resonators as long as near-field interactions between unit cells can be safely neglected, or even for different type of waves such as acoustic or elastic waves.

References

1. Soljacic, M. & Joannopoulos, J. D. Enhancement of nonlinear effects using photonic crystals. *Nature Mater.* **3,** 211–219 (2004).

2. Duchć, D. *et al.* Slow Bloch modes for enhancing the absorption of light in thin films for photovoltaic cells. *Appl. Phys. Lett.* **92,** 1–4 (2008).

3. Painter, O. *et al.* Two-Dimensional Photonic Band-Gap Defect Mode Laser. *Science* **284,** 1819–1821 (1999).

4. Lodahl, P., Driel, A. F. Van, Nikolaev, I. S. & Irman, A. Controlling the dynamics of spontaneous emission from quantum dots by photonic crystals. *Nature* **430,** 8–11 (2004).

5. Joannopoulos, J. D., Johnson, S. G., Winn, J. N. & Meade, R. D. *Photonic Crystals: Molding the Flow of Light (Second Edition)*. (Princeton University Press, 2008).

6. Krauss, T. F. Why do we need slow light ? *Nature Photon.* **2,** 448–450 (2008).

7. Baba, T. & Kondo, K. Dynamic Control of Slow Light Pulses in Photonic Crystal Waveguides. *Transparent Opt. Networks (ICTON), 2014 16th Int. Conf. on, IEEE* 1–4 (2014).

8. Ek, S. *et al.* Slow-light-enhanced gain in active photonic crystal waveguides. *Nat. Commun.* **5,** 5039 (2014).

9. Yablonovitch, E. *et al.* Donor and acceptor modes in photonic band structure. *Phys. Rev. Lett.* **67,** 3380–3383 (1991).

10. Miller, D. A. B. Fundamental limit to linear one-dimensional slow light structures. *Phys. Rev. Lett.* **99,** 1–4 (2007).

11. Safavi-Naeini, A. H. *et al.* Electromagnetically induced transparency and slow light with optomechanics. *Nature* **472,** 69–73 (2011).

12. Hau, L. V., Harris, S. E., Dutton, Z. & Behroozi, C. H. Light speed reduction to 17 metres per second in an ultracold atomic gas. *Nature* **397,** 594–598 (1999).

13. Yariv, A., Xu, Y., Lee, R. K. & Scherer, A. Coupled-resonator optical waveguide: a proposal and analysis. *Opt. Lett.* **24,** 711–713 (1999).

14. Morichetti, F., Ferrari, C., Canciamilla, A. & Melloni, A. The first decade of coupled resonator optical waveguides: bringing slow light to applications. *Laser Photon. Rev.* **6,** 74–96 (2012).

15. Scheuer, J., Paloczi, G. T., Poon, J. K. S. & Yariv, A. Coupled Resonator Optical Waveguides Toward the Slowing & Storage of Light. *Opt. Photonics News* **16,** 36–40 (2005).

16. Notomi, M., Kuramochi, E. & Tanabe, T. Large-scale arrays of ultrahigh-Q coupled nanocavities. *Nature Photon.* **2,** 741–747 (2008).

17. Matsuda, N., Kuramochi, E., Munro, W. J., Notomi, M. & Takesue, H. An on-chip coupled resonator optical waveguide single-photon buffer. *Nat. Commun.* **4,** 1–7 (2013).

18. Vlasov, Y. A., Hamann, H. F. & Mcnab, S. J. Active control of slow light on a chip with photonic crystal waveguides. *Nature* **438,** 65–69 (2005).

19. Yanik, M. F. & Fan, S. Stopping light all optically. *Phys. Rev. Lett.* **92,** 083901 (2004).

20. Baba, T. Slow light in photonic crystals. *Nature Photon.* **2,** 465–473 (2008).

21. Lemoult, F., Fink, M. & Lerosey, G. Revisiting the wire medium: an ideal resonant metalens. *Waves in Random and Complex Media* **21,** 591–613 (2011).

22. Lemoult, F., Fink, M. & Lerosey, G. Far-field sub-wavelength imaging and focusing using a wire medium based resonant metalens. *Waves in Random and Complex Media* **21,** 614–627 (2011).

23. Lemoult, F., Lerosey, G., de Rosny, J. & Fink, M. Resonant Metalenses for Breaking the Diffraction Barrier. *Phys. Rev. Lett.* **104,** 203901 (2010).

24. Belov, P. A., Simovski, C. R. & Ikonen, P. Canalization of subwavelength images by electromagnetic crystals. *Phys. Rev. B* **71,** 193105 (2005).

25. Belov, P. A. & Silveirinha, M. G. Resolution of subwavelength transmission devices formed by a wire medium. *Phys. Rev. E* **73,** 56607 (2006).

26. Shvets, G., Trendafilov, S., Pendry, J. B. & Sarychev, A. Guiding, focusing, and sensing on the subwavelength scale using metallic wire arrays. *Phys. Rev. Lett.* **99,** 53903 (2007).

27. Kaina, N., Lemoult, F., Fink, M. & Lerosey, G. Negative refractive index and acoustic superlens from multiple scattering in single negative metamaterials. *Nature* **525,** 77–81 (2015).

28. Lemoult, F., Kaina, N., Fink, M. & Lerosey, G. Wave propagation control at the deep subwavelength scale in metamaterials. *Nature Phys.* **9,** 55–60 (2013).

29. Liu, Z. *et al.* Locally Resonant Sonic Materials. *Science* **289,** 1734–1736 (2000).

30. Cowan, M. L., Page, J. H. & Sheng, P. Ultrasonic wave transport in a system of disordered resonant scatterers: Propagating resonant modes and hybridization gaps. *Phys. Rev. B* **84,** 94305 (2011).

31. Kaina, N., Lemoult, F., Fink, M. & Lerosey, G. Ultra small mode volume defect cavities in spatially ordered and disordered metamaterials. *Appl. Phys. Lett.* **102,** 144104 (2013).

32. Gao, Z., Gao, F. & Zhang, B. Guiding, bending, and splitting of coupled defect surface modes in a surface-wave photonic crystal. *Appl. Phys. Lett.* **108,** 041105 (2016).

33. Hao, R. *et al.* Improvement of delay-bandwidth product in photonic crystal slow-light waveguides. *Opt. Express* **18,** 16309–16319 (2010).

34. Mekis, A. *et al.* High Transmission through Sharp Bends in Photonic Crystal Waveguides. *Phys. Rev. Lett.* **77,** 3787–3790 (1996).

35. Bayindir, M., Temelkuran, B. & Ozbay, E. Tight-binding description of the coupled defect modes in three-dimensional photonic crystals. *Phys. Rev. Lett.* **84,** 2140–3 (2000).

36. Xia, F., Sekaric, L. & Vlasov, Y. Ultracompact optical buffers on a silicon chip. *Nature Photon.* **1,** 65–71 (2006).

37. Poon, J. K. S., Zhu, L., Derose, G. A. & Yariv, A. Transmission and group delay of microring coupled-resonator optical waveguides. *Opt. Lett.* **31,** 456–458 (2006).

38. Kuramochi, E. *et al.* Ultrahigh-Q photonic crystal nanocavities realized by the local width modulation of a line defect. *Appl. Phys. Lett.* **88,** 41112 (2006).

39. Williams, C. R. *et al.* Highly confined guiding of terahertz surface plasmon polaritons on structured metal surfaces. *Nature Photon.* **2,** 175–179 (2008).

40. Hibbins, A. P., Evans, B. R. & Sambles, J. R. Experimental Verification of Designer Surface Plasmons. *Science* **308,** 670–672 (2005).

41. Fernández-Domínguez, A. I., Moreno, E., Martín-Moreno, L. & García-Vidal, F. J. Terahertz wedge plasmon polaritons. *Opt. Lett.* **34,** 2063–2065 (2009).

42. Gao, Z. & Zhang, B. Broadband wave manipulation in surface-wave photonic crystal. *ArXiv e-prints* 1–11 (2016).

Acknowledgements

This work is supported by LABEX WIFI (Laboratory of Excellence within the French Program "Investments for the Future") under references ANR-10-LABX-24 and ANR-10-IDEX-0001-02 PSL* and by French National Research Agency under reference ANR-13-JS09-0001-01. N.K. acknowledges funding from French “Direction Générale de l’Armement”.

Author Contributions

G.L. proposed the concept and supervised the study. N.K. performed the simulations and the experiments. T.B. developed the metallization process. N.K., A.C., Y.B. and T.B. fabricated the sample. G.L. and N.K. wrote the manuscript. All authors discussed the results and commented on the manuscript.

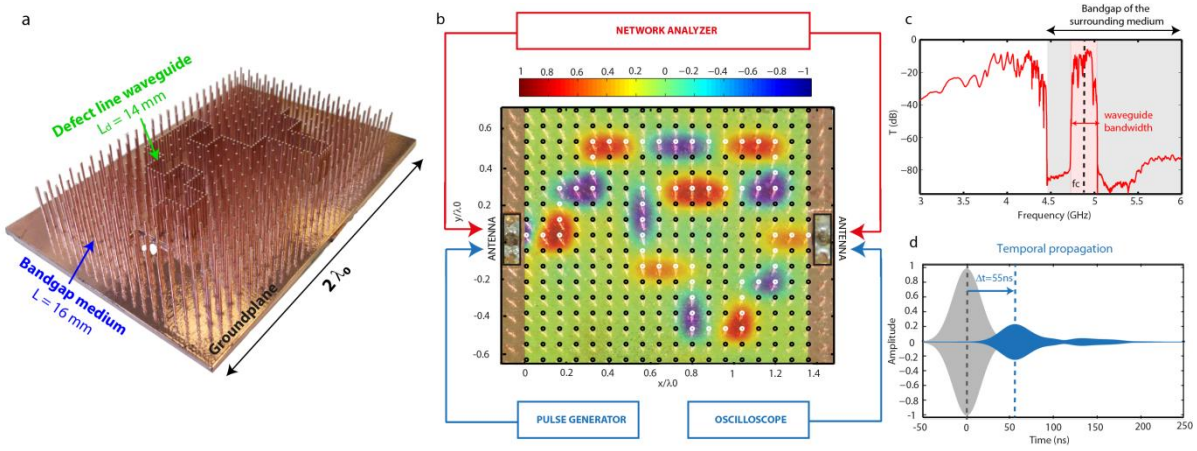

Figure 1| Subwavelength waveguiding demonstration in a tortuous metamaterial waveguide. a. Photograph of a 3D printed and chemically metallized wire array sitting on a ground plane comprising a tortuous defect line made out of shorter wires. To highlight the presence of the defect line, we represent in this picture a waveguide with defects separated by ag=1.5 mm, a distance three time smaller than in the sample we actually investigated the properties. **b,** Real part of the experimental E-field at f = 4.795 GHz, mapped in superimposition with a top view of the photograph of the device. Dark circles represent wires in the surrounding medium while white ones highlight the defects waveguide path. Schematic representation of the measurement set-up for the spectral (resp. temporal) properties in red (resp. blue). **c**, Spectrum of the transmission (dB). **d**, Temporal propagation of a 20 MHz wide pulse centered on f_c with both emitted (grey) and received pulses (blue).

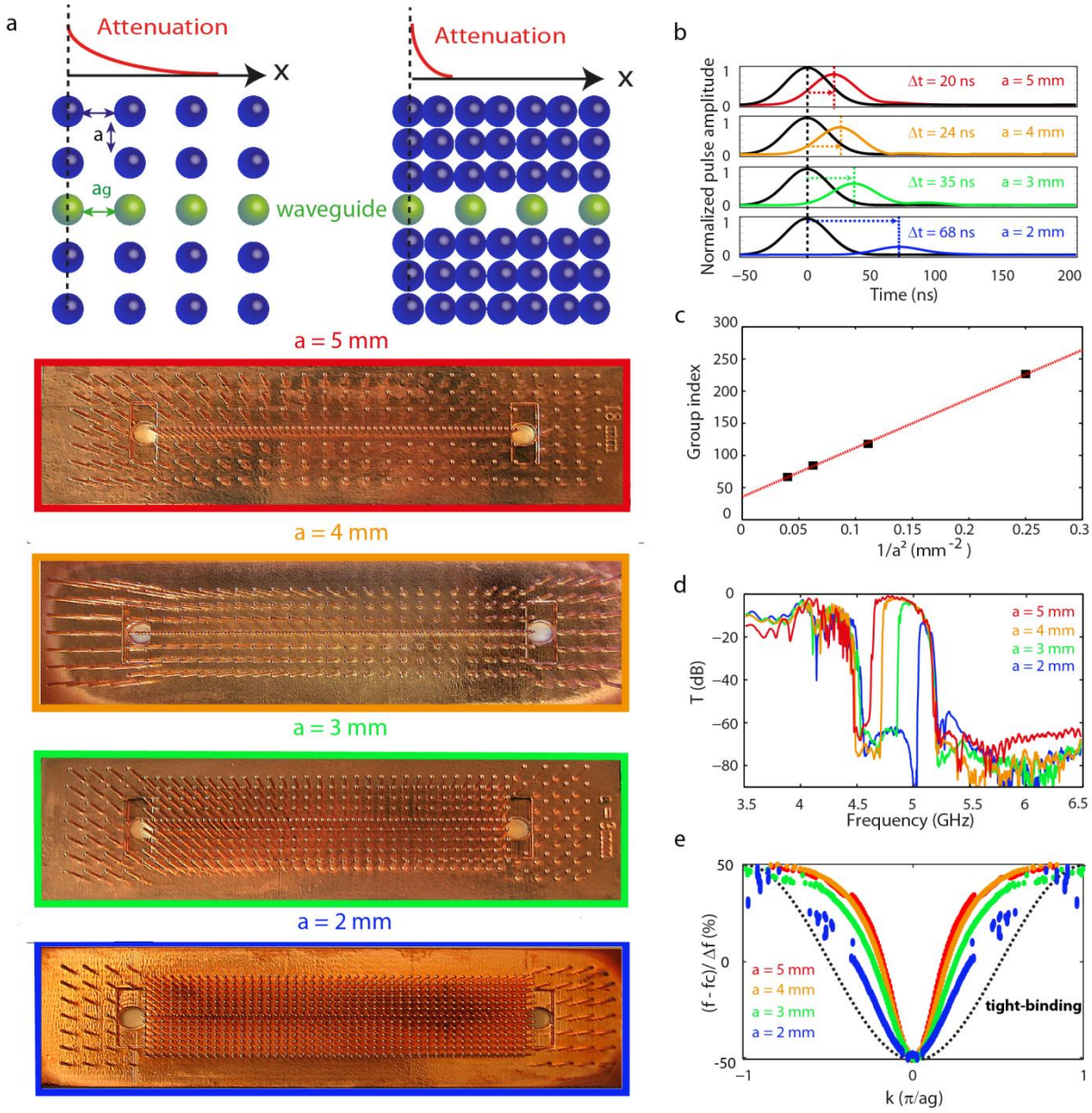

Figure 2| Effect of the bandgap medium density on the transmission properties of the slow wave line defect waveguides. a, Schematic representation of waveguides embedded in a bandgap medium with different densities and photographs of the four investigated devices. **b-e** Experimental results for all samples with densities ranging from a = 2 mm to a = 5 mm comprising: **b**, the envelope of the sent (black) and propagated (color) pulses at central frequency f_c, **c**, the group index at central frequency f_c as a function of $1/a^2$, **d**, the transmission spectra (dB) and **e**, the dispersion relations displayed with normalized wavenumbers and with the frequency centered on the central frequency and normalized by the bandwidth for each waveguide. .

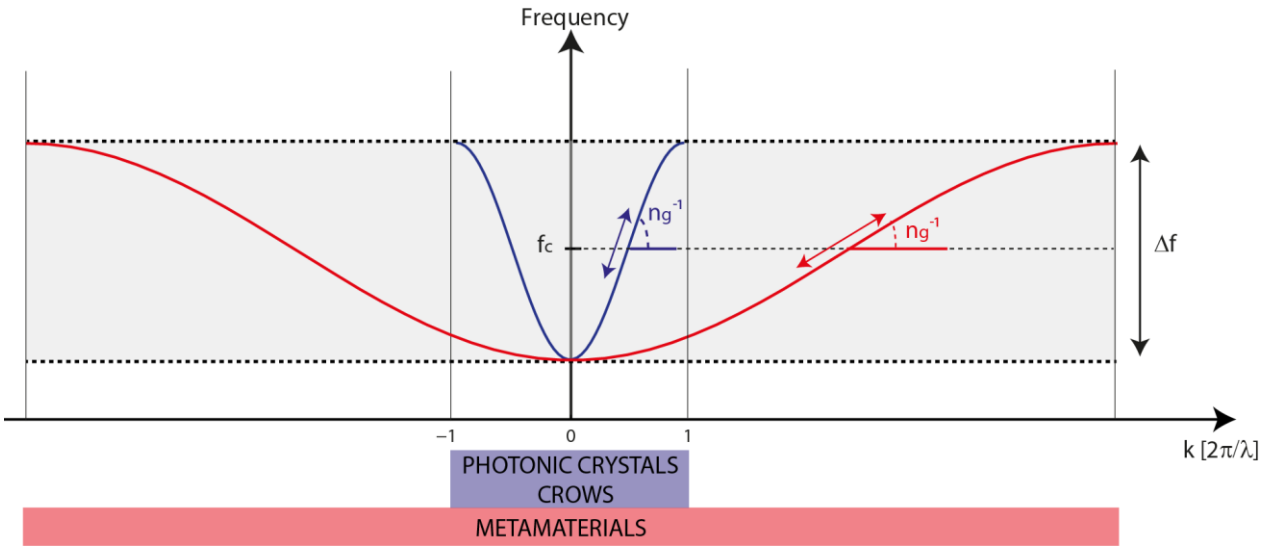

Figure 3|Schematic tight-binding dispersion relations for two chains of coupled cavities with different waveguide periodicities a_g. Dispersion relation for a typical periodicity in photonic crystals coupled cavities waveguide or CROWS that is the order of the wavelength at resonance (blue) and for a subwavelength period as it is the case in metamaterials (red).

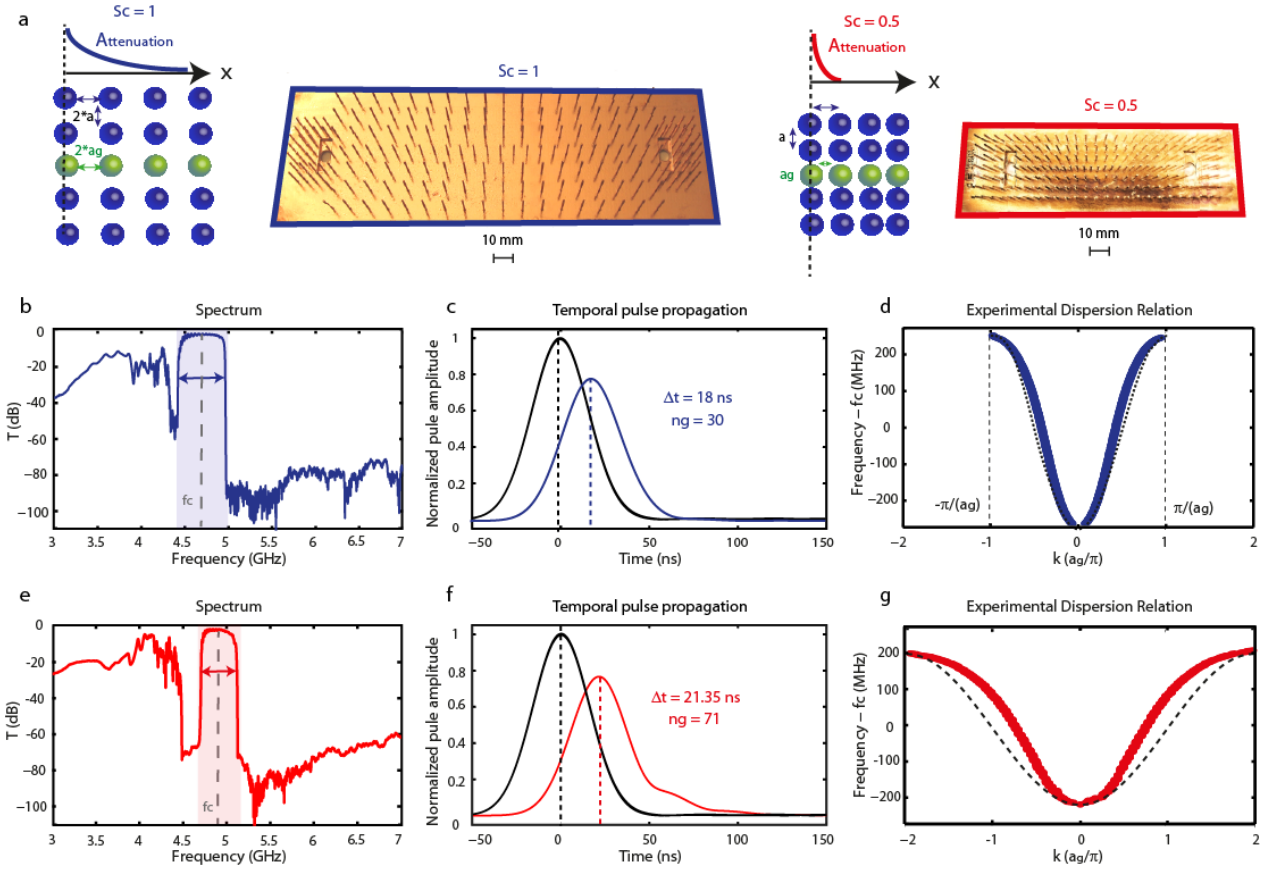

Figure 4| Effect of the device scaling on the transmission properties of the slow wave line defect waveguides. a, Schematic representations and pictures of the scaled samples Sc = 1 (left) and Sc = 0.5 (right). **b-d** Transmission spectrum (dB), envelope of the sent (black) and propagated (color) pulses at central frequency f_c and profiles of the dispersion relations along with the theoretical tight-binding model (dotted black) for the Sc = 1 sample. **e-g** Same for the Sc = 0.5 sample. The wavenumbers in **d** and **g** are normalized by the waveguide periodicity a_g in the sample Sc = 1.

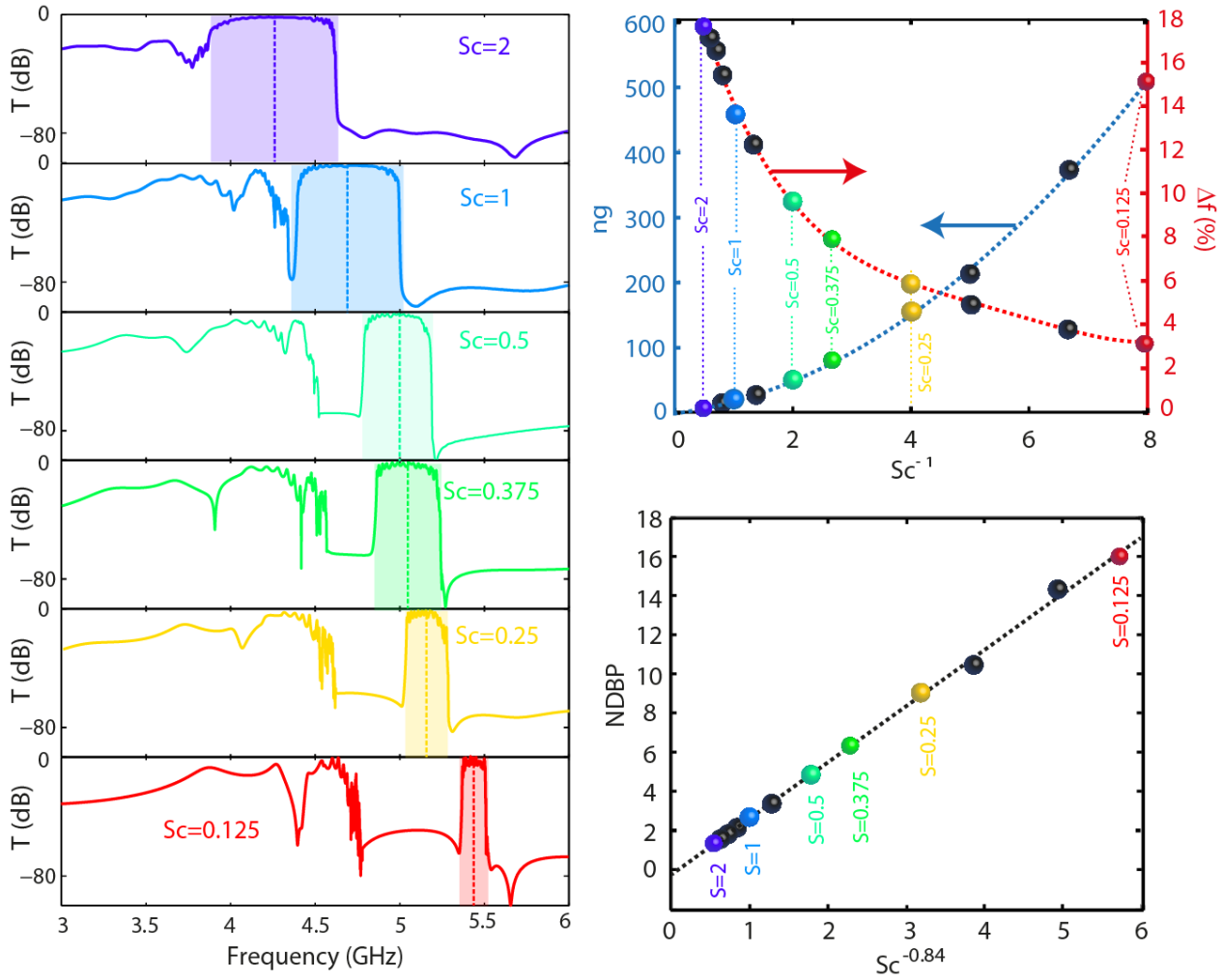

Figure 5| Simulation of the effect of the sample scaling on the delay-bandwidth products of the slow wave line defect waveguides. a, Simulated transmissions (dB) for six out of twelve devices with scaling factors from Sc = 2 to Sc = 0.125. **b** Evolution of the group index n_g at the central frequency (y-axis left in blue, dotted blue line and black points) and the transmission bandwidth in % of the central frequency (y-axis right in red, dotted red line and black points) as a function of the inverse of the scaling factor 1/Sc. The colored points on the two curves correspond to the values of scaling factors represented in **a**. **c**. Normalized delay-bandwidth product as a function of $Sc^{-\alpha}$, where α=0.84 gives a linear dependence. Black dotted line is the linear fit and colored points correspond to the values of scaling factors represented in **a**.

SUPPLEMENTARY INFORMATION for

Slowing down waves in locally resonant metamaterials line defect waveguides

1. **Device fabrication**

The samples are 3D printed in an ABS-like polymer resin using an Objet30 Pro 3D printer. The surface of the polymer is first annealed then submitted to an acidic treatment to produce chemical functions for the copper metallic ions chelation. The latter are chemically reduced to create copper nanoparticles or clusters onto the surface that acts as a seed layer catalyzing the copper electroless plating. To reach the copper bulk electrical properties and hence minimize the dissipation of waves in the polymer matrix, the thickness of the copper electroless plated layer is further increased over 20 µm by performing copper electroplating of the resulting conductive samples. Thickness and surface morphology of the plated copper layers were examined with a SEM, scanning electron microscope, (JSM-5510LV, JEOL, Tokyo, Japan). Wires of the metamaterial were cryo-fractured with liquid nitrogen to probe the height of the copper layer. SEM micrographs of the wire slice were taken at various magnifications ranging from 100× to 5 000× (X300 displayed in Fig. S1) applying the secondary electron detector. The acceleration voltage and working distance were respectively 4 kV and 17 mm. From Figure S1, we clearly observe that the copper layer is between 20 µm and 50 µm high, largely over the copper skin depth at 5 GHz (0.92 µm).

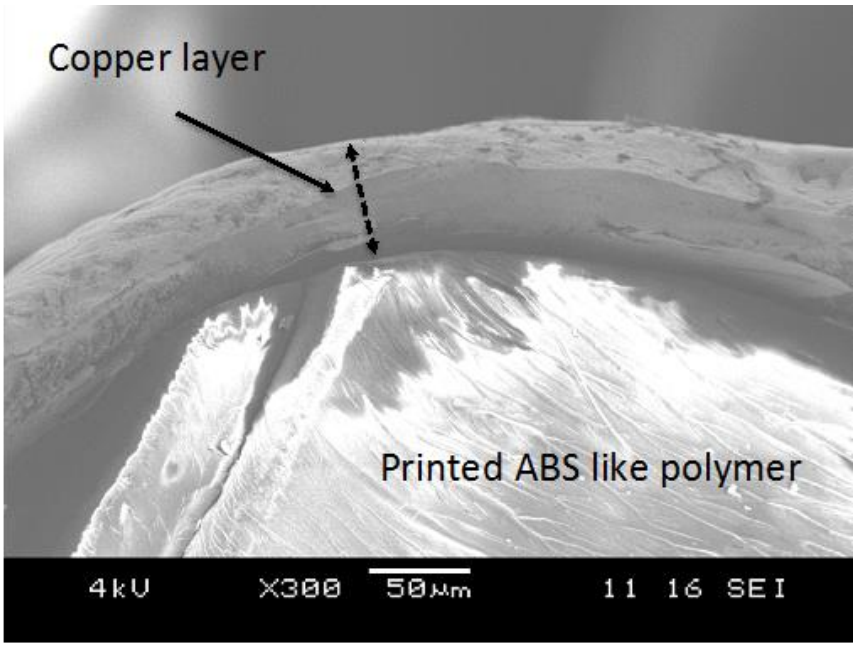

Figure S1| SEM image of a part of a section of a polymer copper coated wire after the whole metallization process.

2. Design of the devices

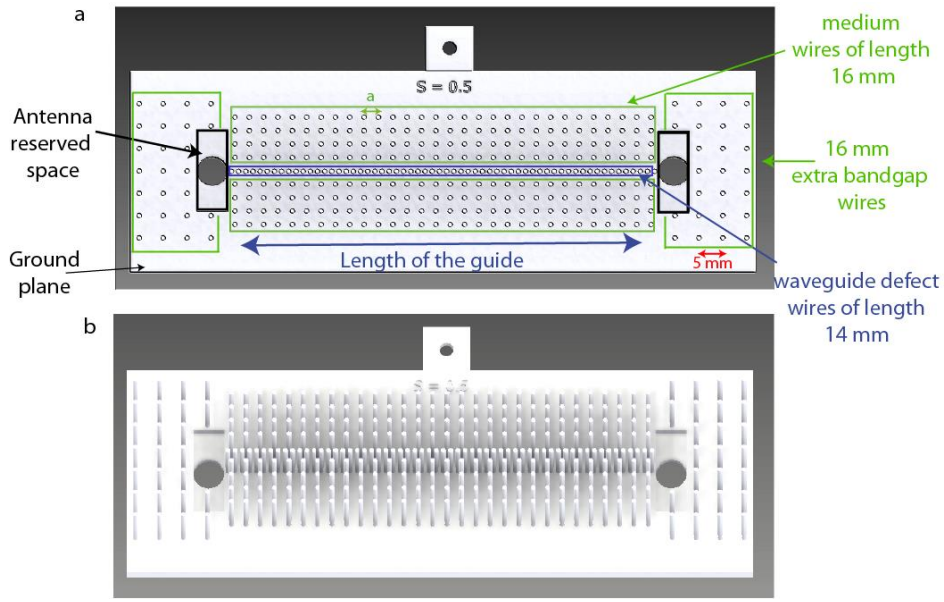

Figure S2| CAO views of a typical device. **a**, top, **b**, perspective

The devices all consist of a ground plane (height = 3 mm, length and width variable) on which two 6.5x18 mm^2 rectangles are extruded, corresponding to the required space to put the antenna base. Within this space, a hole is drilled to insert the SMA connector so that the electrical wires for the measurements are connected below the ground plane. The wires of the medium (green in Fig. S2) are all of length L = 16 mm and surround the waveguide in the whole space between the antennas. The period *a* of this medium depends on the device and varies from 2 mm to 10 mm. The waveguide is composed of N (60 for the devices of Figure 3, 26 for the ones of Figure 4) wires of length L_d = 14 mm, separated by a distance a_g (from 1.5 mm to 6.97 mm). All the wires are 1 mm wide, which is limited by the resolution of the 3D printer to grow wires with conformal width on such heights. Some extra wires of length L (green in Fig. S2) arranged on a 5 mm lattice are added behind the antennas in order to provide a bandgap medium at the waveguide transmission band frequencies, so that the antennas are isolated from the exterior. It then insures noise limited measurements.

3. Simulation of the transmission through the tortuous waveguide

Using the software CST Microwave studio, we simulate the transmission through a sample analogous to the experimental tortuous waveguide of the figure 1 in the main text. The S-parameter through the waveguide is displayed in figure S3 (red). We observe the same form of transmission spectrum as in the experiment, with low frequency modes and a bandgap attributed to the environing wire medium and a transmission band around 5 GHz. To demonstrate that this transmission band is indeed the signature of the transmission through the line defect waveguide, we furthermore simulate the same devices but with the wires that all have the same length (as schemed in figure S3)., that is that we suppress the line defect waveguide. The transmission, in black, confirms that the transmission band disappears and that only the bandgap of the medium remains for this frequency range.

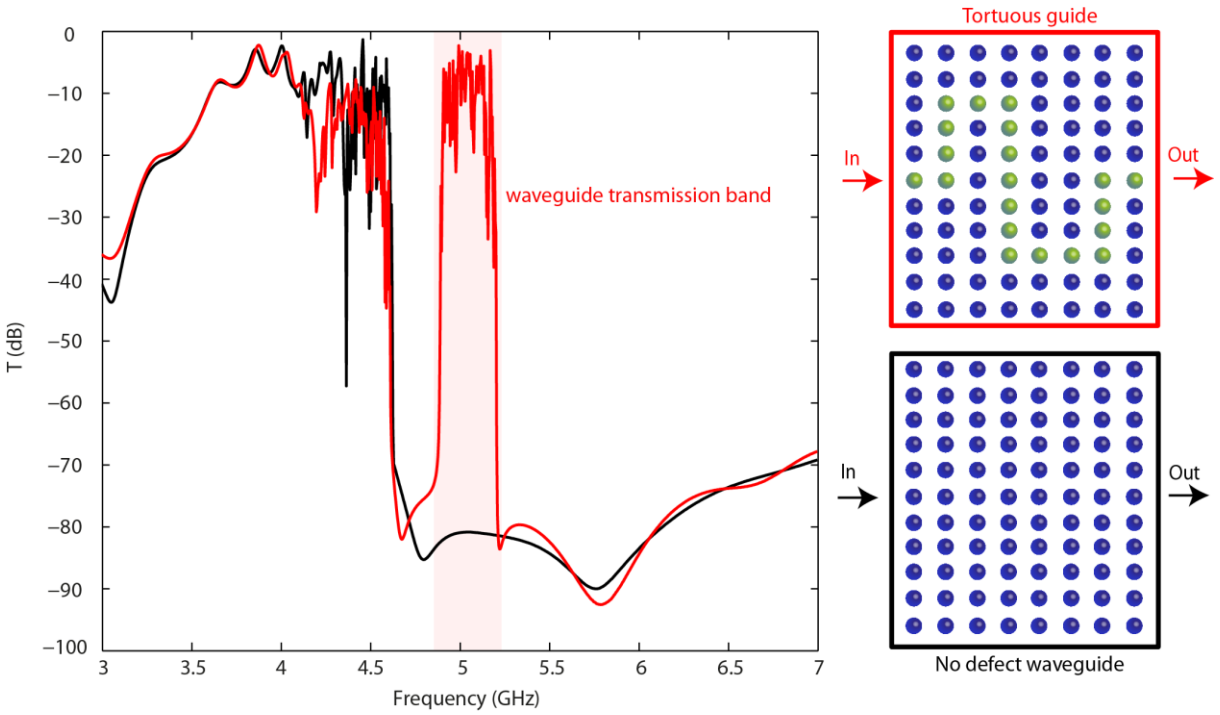

Figure S3|Simulated transmission through the tortuous waveguide of Figure 1. Simulated transmission through the waveguide (red) and through the medium with no defect line waveguide (black) along with schematics of the two simulated devices (blue dots = wires of the medium, green dots = defect wires).

4. Experimental setup

a. Spectral and temporal measurements

Home-made antennas were used for all measurements (Fig. S4). In both spectral and temporal measurements, the antennas consisted of cut stain wires soldered on SMA connectors. The length of the antenna wires was manually adapted in order to get the best possible coupling to the waveguide, that is the highest transmission (considering the losses) and the minimum oscillations (typical of reflections). The length was set to 21 mm. The antennas were placed at the designed spot within the device at each side of the waveguide, around 4 mm away from the first wire of the waveguide, distance which is limited by the width of the SMA base. Since this distance partly drives the coupling to the waveguide (the further, the lower the coupling), we soldered a stain wire of length 14 mm (same as for the defects) on the base of the SMA so that it decreases the distance in-between the antenna and the first wire.

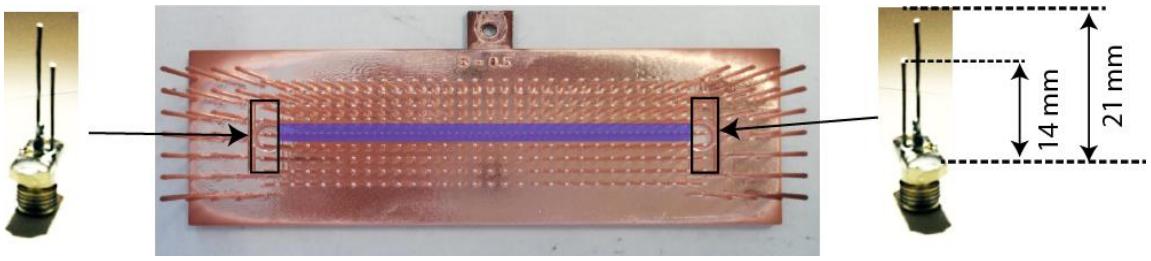

Figure S4| Picture of a device and of the home-made antennas. The waveguide defect wires are highlighted in blue and the holes for antennas in solid black rectangles. Photographs of the home made antennas used for spectral and temporal measurements with the feed antenna of 21 mm and the extra defect wire of 14 mm (sides).

Spectral measurements were conducted while connecting both antennas to a beforehand calibrated network analyzer (Agilent Technologies N5230C) for frequencies ranging from 3 GHz to 7 GHz. Each measure was averaged 10 times. As for the temporal measurement, one of the antennas was connected to a waveform generator (Tektronix AWG7102, 20 GS/s when interleaving channels) thus acting as a source, while the second was connected to an oscilloscope (Tektronix TDS6604B, 20GS/s). In order to probe the properties over the whole bandwidth of the waveguide, we sent for each device a wide pulse centered on the latter central frequency. The measurements were then filtered on a 20 MHz bandwidth for 200 different frequencies within the waveguide transmission band (results are displayed on Fig. S6). The group index for each frequency was retrieved from the delay between the sent and received filtered pulses. It was measured from the maxima of the envelope of those pulses while the reference velocity was taken as $3e^8$ m/s. The amplitudes of the pulses were normalized to the maximum of amplitude of the input pulses.

b. Dispersion relation measurements and mode mapping

To measure the dispersion relations (resp the map of the E-field), we scan the E-field on a line along the waveguide from the first wire to the last one (resp. above the entire area above the whole sample), around 1 mm away from the top of the wires, with a step of $a_g/4$. The waveguide is fed by one of the previously described antenna connected to one port of the network analyzer. The field probing is implemented with a home-made antenna consisting of a very short, hence inefficiently radiative to preferentially probe the evanescent field, stain wire mounted on a SMA connector plugged to the second port of the network analyzer. This antenna is mounted on a 2D translational stage (Newport M-IMS400PP). In order to prevent from reflections at the end of the waveguide that would create

stationary waves, the second antenna in the sample is maintained (Fig. S5) but loaded with a 50 Ω load. To determine the dispersion curves, a spatial Fourier transform of the acquired spectra for each position was performed. For each frequency, the wavevector with the maximum contribution in the FFT is kept to plot the dispersion curves as they are presented in the main text.

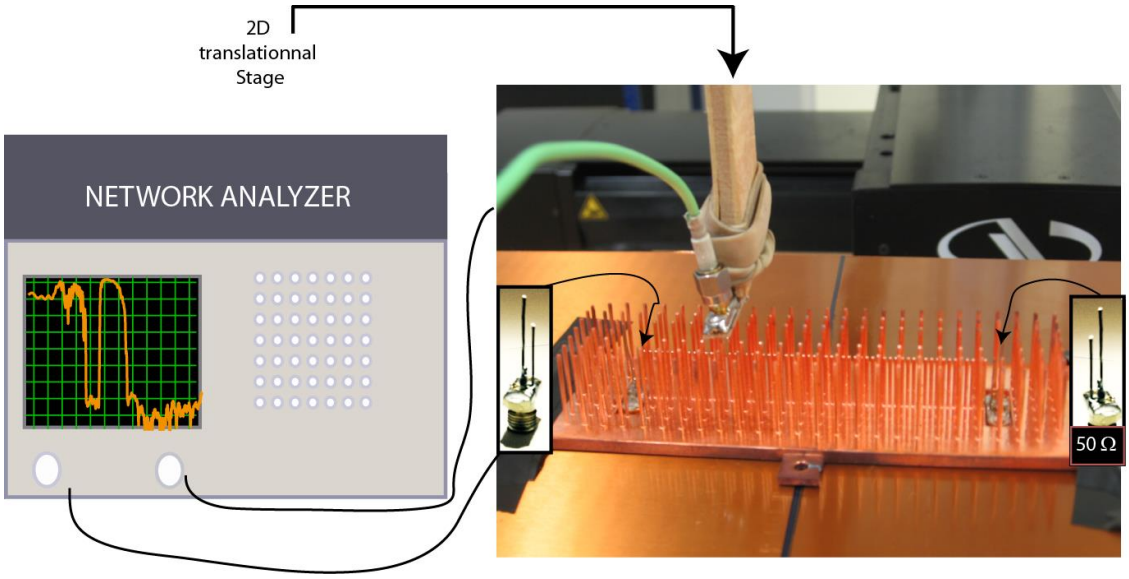

Figure S5| Setup for the measurements requiring scanning of the E-field over the device.

5. Supplementary experimental results: Wide band temporal measurement

We know from the shape of the dispersion relation, relatively similar to a tight-binding one that the group index consequently varies within the waveguide transmission band. For the sake of clarity, in the main text, we restrained our measurement to n_g around central frequencies (averaged over 20% of the bandwidth, see shaded areas in Fig. S6) though it was obvious it would give the lower delays. The group index indeed dramatically increases at the edges of the band where the dispersion curve flattens.

The group index while plotted on the whole frequency range shows that much higher values can be reached by changing the operating frequency (up to 300 for a = 2 mm dense medium) as displayed in Figure S6a. Of course, the group index enhancement will lead to an increase of the transmission losses, so that there is a trade-off to find to get the most efficient delay lines.

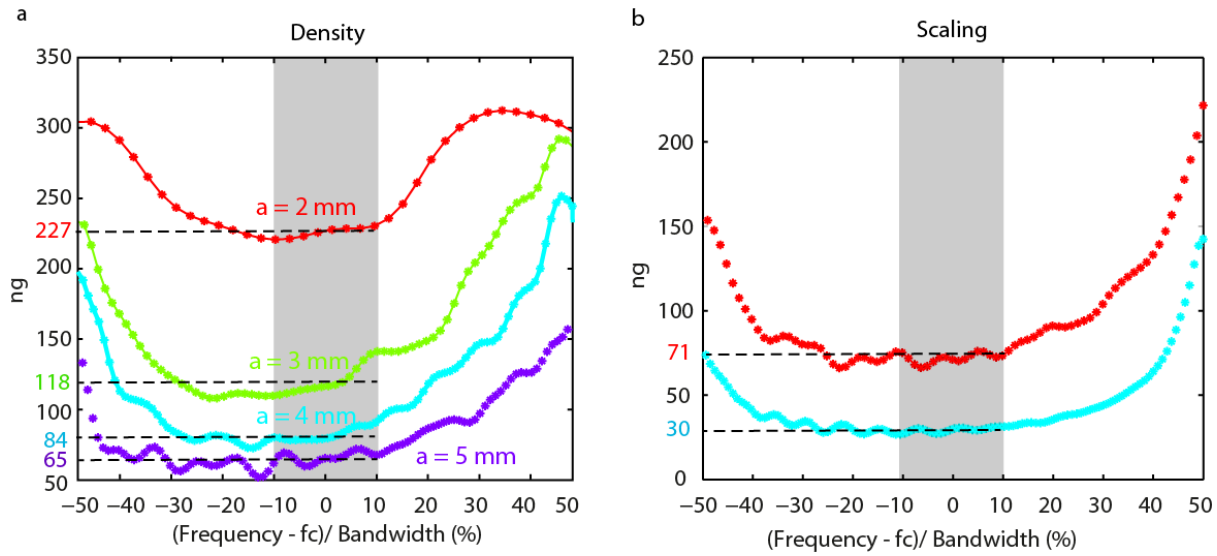

Figure S6| **Experimental broadband measurements of the group index. a,** samples of Figure 3a and **b**, samples of Figure 4b. Data are plotted as a function of the frequency, centered on f_c and normalized by the bandwidth. The x-axis is presented as a percentage of the bandwidth. The frequency range on which the group index displayed in the main text is averaged is shaded in grey, while the corresponding value is advised on the y-axis.

We furthermore emphasize that this curves are not entirely symmetric since our dispersion relations are not purely tight-binding but display some features of a polariton. Particularly, the group index is higher at the upper edge of the band, where the dispersion gets to its flat asymptote which is characteristic of polaritonic dispersion relations. Finally, we observe that the larger the periodicity of the medium, the larger the bandwidth on which the group index is relatively constant, that is the bandwidth with linear dispersion.